DATA-DRIVEN ANALYSIS OF AIRCRAFT TOUCHDOWN PATTERNS ON AIRPORT RUNWAYS USING SATELLITE IMAGE PROCESSING TECHNIQUES

Mohammed Ba Zuhair[1], Volker Gollnick[1], Florian Linke[2], Alexander Lau[2]
[1]Hamburg University of Technology, Institute of Air Transportation Systems, Hamburg, Germany
[2]German Aerospace Center, Institute of Air Transportation Systems, Hamburg, Germany
mohammed.ba.zuhair@tuhh.de, volker.gollnick@tuhh.de, florian.linke@dlr.de, alexander.lau@dlr.de

Abstract

This paper presents an image processing-based method for analyzing satellite scans taken from 24 airports and runways different in size and location to detect and understand variations in landing behaviors by extracting aircraft wheels rubber spots deposited in runway touchdown zones. The analysis establishes a clear correlation between the observed rubber material distributions and the locally or globally governing operational constraints, showing for instance the effect of the ongoing pandemic or noise abatement procedures on the change of landing behaviors in some European airports. Statistical generalizations are also suggested and combined with an explanatory Monte Carlo model under Gaussian Processes considerations. In addition, the identified change in landing manners is correlated with runway landing operations efficiency in the short and long terms. The paper also provides examples of the proposed method applications that may be of potential value for both aircraft and airport operators.

Key words

Image processing, touchdown, aircraft approach, landing operations, runway

1. INTRODUCTION

Among the most important objectives of capacity-constrained airports is the constant pursuit to improve runway operations efficiency [1]. When related to landing operations, runway efficiency is dependent on the Arrival Runway Occupancy Time (AROT). This is typically defined as the time an aircraft consumes to travel the distance from the threshold to the assigned exit on a specific runway. Accordingly, this process can be divided into the following main phases: approach, touchdown, and braking. The two initial phases describe aircraft motion along a trajectory that starts from a predefined point floating over the runway threshold, ideally at 15m, until fully contacting, i.e. using all wheels, with runway surface within the so-called touchdown zone. Due to the intrinsic stochasticity of landing operations, actual landing phases and the total AROT are considerably variable, which however, is found to be mainly determined by the arriving aircraft type and the assigned runway exit parameters [1]. To enhance landing quality and runway occupancy process efficiency, systems, methods, and procedures that aid in understanding the governing initial landing behaviors and regulating their outcomes are of particular importance and influence. This significance gains more relevance as regulations towards shorter wake vortex separations are gradually coming into effect in many airports worldwide imposing stronger limitations on the allowable AROTs [2-3].

In general, works dealing with data-driven analysis of landing processes can be categorized into two main domains. In the first domain, studies use flight recorder information or surveillance system data as in [2, 4-6]. Although these data sources ensure high quality and reliability, they require authorized accessibility to essential proprietary databases. In reality, this constrains the ability to conduct large-scale data-driven investigations to the major regulatory or research centers in the aeronautical community. Despite being an alternative new free data source, Automatic Dependent Surveillance - Broadcast (ADS-B) flight data have proven themselves inappropriate for pinpointing exact touchdown locations due to the relatively long signaling buffers [7]. On the other hand, the second domain of the data-driven studies relies on image analysis methods to detect airports or recognize their runways graphical objects [8-10]. Here, two ways of image acquisition can be recognized, one of which applies real-time image generation and analysis using embedded vision and guidance systems to enable autolanding capabilities [11-13]. Accordingly, this way is limited in use and accessibility. The other way benefits from the freely-accessible and abundant satellite image database with the aim of automatic airfield identification and localization [14-17]. In this regard, techniques of satellite image processing are used to recognize airport geometric and surface texture features to enable their automatic classification and targeting.

In this paper, a novel approach is proposed to explore touchdown zone rubber spots and patterns that can be seen in freely-accessible satellite digital images via GoogleEarth Pro interface [18] for extending our understanding of piloting and transport aircraft landing behaviors on different airports and runways.

2. ANALYSIS METHODOLOGY

To achieve the study goal, the method suggests simple and effective image processing procedures to utilize satellite

zoomed-in static runway scans through the identification, extraction, and segmentation of main and nose wheels rubber black points and tracks scattered on the touchdown zone surface. These points are typically deposited on the pavement during every touchdown and braking event. Therefore, touchdown zone satellite scans may represent a high-resolution and valuable digital information that can be analyzed to derive new operational implications.

2.1. Database build-up and pre-processing

To capture touchdown zone rubber patterns, a representative set of 24 different local and international airports is selected as listed in Table 1. For every airport, a manual process to search and collect tens of historical satellite images was conducted. As shown in Fig. 1, this process began with pinpointing EDDF airport geographic location using public location data, which is then followed by the identification of its arrival runways using direct historical and visual observations or published airport specifications. Finally, dimensions of the touchdown zone were determined using a generalized procedure that considers snipping only the part of runway image that contains all landing markings as clearly seen in Fig.1 to the left side. This snipped segment of the runway is equal to 880-900m in terms of length units. In the process of airports selection and associated images sampling and database buildup, the following criteria were also strictly considered to ensure high-quality and relevant data:

1) *Size and geographic location*. Runway efficiency is basically the interest of large and congested airports, therefore, they are increased in quantity and diversified in size and geographic locations in the sampled dataset.
2) Surrounding operational factors. Parameters of the investigated initial landing process is influenced by the surrounding terrain and dominant weather factors. Thus, it was interesting to include airports located in the neighborhood of large terrains or constrained by water boundaries, e.g. TNCM and LOWI, to explore any correlations between such boundary atmospheric and geographic conditions and resulting touchdown patterns.
3) Data availability and quality. Although the vast majority of civil airports can be observed in satellite images, the challenge of collecting sufficient images cannot be underestimated. Thus, it is reasonable to set preliminary image selection rules that facilitate acquisition and subsequent effective image enhancement and segmentation using moderate computational power and time requirements. In result, runway images that suffer from eye-catching distortions or clear blurring as exemplified in Fig. 2(a) are excluded. Also, images containing clouds or their shadows on runway surface are deemed defected. Furthermore, the executed sampling campaign has established that most old satellite scans suffer from limited resolution that may penalize subsequent segmentation process. Therefore, satellite scan dates are limited to 2010. For new airports and runways that were built after this time limit, runway pavement and construction completion date was the starting date of scans sampling. On the other hand, high illumination and contrast in the images is of major interest. Sometimes, pavement repairs and padding activities can unfortunately result in dark black color spots that blend inner or neighboring rubber stains. In some cases, they are indistinguishable even for the human eye, e.g. Fig. 2(b). Therefore, such images were sorted out as well. This is also relevant to images with runway objects, e.g. aircraft and trucks, that are occasionally seen, shadows of which cause strong undesired deviations or spikes of black color spatial concentrations, e.g. Fig. 2(c).

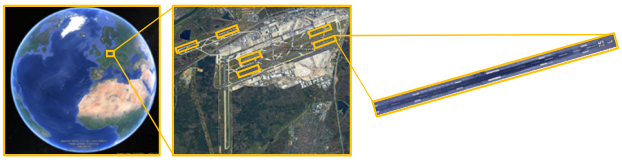

FIG. 1: Process of an airport localization, arrival runways identification, and touchdown zone extraction

The conducted satellite scans sampling process generated over 600 images from the selected airports, 6% of which was filtered out according to the described above filtering and cleanup criteria. In general, busy and hub airports enjoy higher coverage and imagery compared to remote and small airports.

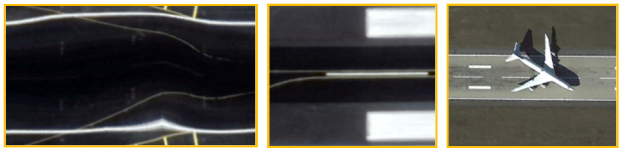

(a) (b) (c)

FIG. 2: Examples of touchdown zone image defects

Tab. 1: ICAO codes of the selected airports

Big airports	*Small airports*	*Steep/short approach airports*
EDDF; IST; KATL; OMDB; KJFK; EGLL; LFPG; LEMD; LEBL; EDDM; LEPA; EDDH; LFPO; LPPT; ZGGG; ZGSZ	TNCM; LPMA; LOWI; VNKT	EDHI; EBLG; LEZL

2.2. Database build-up and pre-processing

At touchdown and before their spinning up, nose and main landing gear tires momentarily drag on the runway unsmooth surface causing significant heating and subsequent melting of some tire tread. This draws rubber points and tracks that can be traced back by observing the characteristic black spots and build-up rubber material layers visible on the touchdown zone. Due to their considerable thickness and lengths along with the remotely visually distinguishable colors, these rubber areas can be identified even at high altitudes, e.g. 3000m. Therefore, knowledge of standard rubber and runway surface colormaps can be utilized to apply morphological and color-based segmentation techniques with the aim of isolating rubber-representing dark grey and black pixels.

This process starts with the exclusion of irrelevant black micropixels typically found around graphical objects such as white and yellow runway designators, landing markings, signs, and taxiway or centerline edges. For this purpose, few morphological operations based on line- and rectangular-based dilation and erosion are conducted after setting the corresponding shape dimensions to carefully defined small limits due to actual smallness of the described runway graphical objects when compared to the runway touchdown zone area.

The obtained distinction between runway color regions enables further thresholding to facilitate separation of pavement and rubber areas. As known, runways are typically characterized by grey-scaled colormap which is indeed used to exclude non-rubber relevant areas. The applicable thresholding factor is experimentally found to be ranging between 0.6 – 0.8 depending on the desired level of black color isolation. Low thresholding factor extracts regions of strong contrast, while higher thresholding factor generates less conservative separations. For consistency and generality, a good approximation favors ~ 0.8 to enable sufficient rubber-representing pixels extraction as shown in Fig. 3 when applied on the Frankfurt am Main airport (EDDF) - runway C25. To convert pixel units to the equivalent distance units, touchdown zone area information collected during the data collection process was considered. Although the majority of rubber material is effectively extracted and its distribution pattern is well-captured, neglection of few scattered rubber points mainly located on runway markings is noticed. This is an expected consequence of the morphological filtering operations and has little influence on the total sum of rubber points.

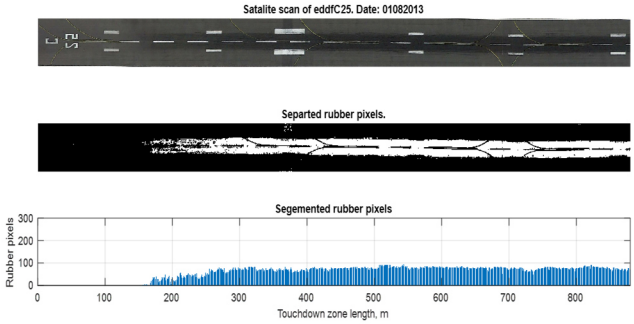

FIG. 3: EDDF C25 runway rubber points extraction and segmentation process results

3. RESULTS

The algorithm implemented to analyze a single touchdown zone image can be further extended to explore multiple runways and airports rubber material patterns and distribution characteristics. To systemize our analysis and observations steps, three-level view of runways sets is suggested. In the first level, rubber points are collected from a single runway only. In the second level, a set of runways located in one airport are investigated. In the third level, a higher perspective is achieved by investigating and comparing grouped runways from different airports to each other.

3.1. Runway-level observations

According to ICAO empirical approximations for modern multiple taxiway runway design, it can be assumed that aircraft within low approach categories (APC), i.e. A and B, travel 250 ± 30m along the runway until touchdown. On the other hand, larger aircraft types, namely C and D, often use 450 ± 50m of the runway length [19]. The introduced deviations emerge from the inevitable influence of the stochastic case-sensitive atmospheric, operational, or geographic factors. In scenarios of minimized transition phase duration under Federal Aviation Regulations (FAR 25) requirements, pilots spend 1-3 sec. after touchdown in order to rotate the aircraft [20], which may add extra 150–250m.

Due to the intrinsic stochastic nature of landing input and output parameters within actual landing scenarios, a rather conceptual and comprehensive modelling method is used to model final approach and touchdown points distribution and patterns. For this purpose, it is reasonable to implement Monte Carlo methods under Gaussian Process Framework. This ensures realistic and relatively inexpensive numerical representations of any large-scale air traffic flow into an arbitrary big airport. The key mathematical description of this process can be represented as follows,

$$L_{i,N} = L_{TD0,i} + \xi_N(1,N) \cdot \Delta L \tag{1}$$

where $L_{TD,i}$ is the mean air distance, or alternatively touchdown location, travelled by an aircraft type within APC i, and $\xi_N(1,N)$ is the samples array of length containing independent random values with the standard Gaussian distribution, and N represents the quantity of landing scenarios, while ΔL is the statistical noise, i.e. deviation, variable. As an example, to model landings under the reported mean L_{TD0} and ΔL above [20], it becomes clear that touchdown points scatter along the touchdown zone as seen in Fig. 4. Note that this assumes an average hourly runway throughput of 30 as suggested by FAA for initial relevant approximations [21]. This is found to generate around N = 1.0×10^6 landings per annum. Here, we see that the empirical mean of all sampled events is located at ~500m from the threshold. As expected, arriving fleets of higher approach speeds, e.g. D, tend to require more air distance compared to the slower aircraft types.

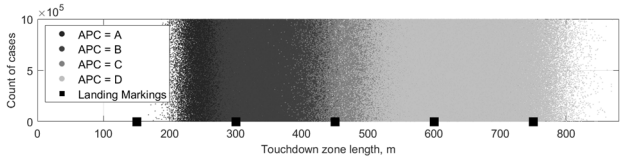

FIG. 4: Typical distribution of touchdown points under statistical and FAR data

Afterwards, it becomes interesting to explore actual touchdown zones by extracting and understanding the obtained dominant rubber patterns and distributions. In this section, we begin with a single runway case, e.g. EDDF 25L, whose rubber points were collected for the time interval 08.01.2013 – 03.07.2021. The selected runway along with the other parallel runways, namely 07C, 07R, and 25C are 4000m long, are operable for arrivals. On the contrary, the new landing runway, 07L and 25R, is only 2800m long and can be therefore assigned only for A-C

aircraft. As presented in Fig. 5, the analyzed historical scans show an overall rubber points (pixels) distribution normality. Older scans than 2020 show local concentrations between 400-600m which lies directly beyond the main landing marking, i.e. 450m. Furthermore, it is obvious that the initial landing phases, i.e. touchdown and rotation, tend to use most of the available touchdown zone, yet with higher preference for delayed touchdowns. More interestingly, it is noticed that landing behaviors and resultant rubber patterns have slightly changed in recent years. In most dates prior to 2020, quantity of rubber points, which is correlated to rubber density, has clearly decreased. The main reason of this observation can be attributed to the dramatic drop in global and European air traffic since early 2020 when the Corona pandemic outspread.

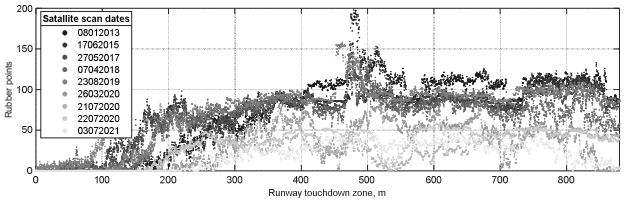

FIG. 5: Historical collections of rubber points observed on the touchdown zone of EDDF 25L

In addition, a time-dependent behavior regarding how short approaches were performed is observed. Analysis of touchdown points located between 0 – 200m shows that most older landings had higher rate of short approaches compared to recent landings. This is another interesting operational observation that can be related to the gradual introduction of few noise abatement procedures at EDDF, some of which obligate pilots to reduce approach noise by conducting final approach from higher altitudes, which slightly prolongs approach phases [22]. Effects of such socio-ecological operational requirements are evident on large and congested airports located in the vicinity of urban areas. For smaller airports, where community concerns with respect to aircraft noise are less, it seems that these airports have no strict noise-related procedures, which allows pilots to follow a normal landing trajectory to the middle region of the touchdown zone as seen for instance in the case of Airbus GmbH airfield in Hamburg, see Fig. 6. Note that this runway is used mainly for Airbus operations-related flights and airfield tests. Also, the effect of putting main landing marking closer to the runway threshold in short runways incentivizes pilots to shorten final flare phase and nose-down (rotation) process and ensures safe landings without overrun hazards. When compared to Fig. 4, an overall good agreement between the observed and statistical APC-wise touchdown points distribution patterns is established.

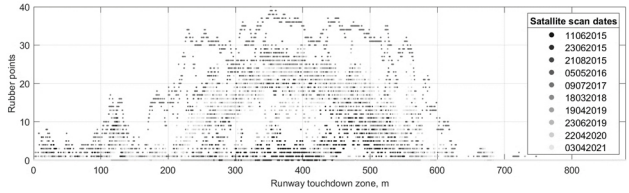

FIG. 6: Historical collections of rubber points observed on the touchdown zone of EDHI 23

3.2. Single airport-level observations

Here, our analysis perspective is further elevated to obtain a better overview on a specific airport. For this, rubber points detectable on all landing runways were collected. To achieve this task, difference in runway directions, i.e. left and right, must be considered when generating the unified view. Therefore, the concatenated images containing right runway thresholds were automatically flipped since runway direction labels were already input during the pre-processing phase. In Fig. 7, we see that the overall shape of rubber points constellation corresponds well to Gaussian distributions with a mean touchdown spot around 500m. Again, time-dependent effects resulting from pandemic consequences coupled with noise reduction measures are evident on a larger scale. In more detail, it is noticed that rubber points have reduced in quantity and are displaced forwards with time progress.

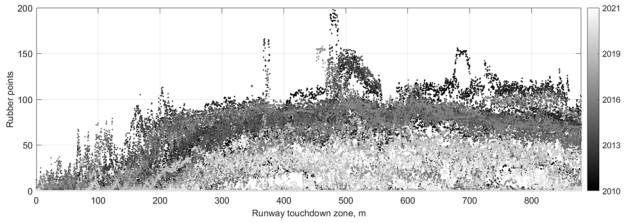

FIG. 7: Historical collections of rubber points observed on all landing runways at EDDF

For purposes of comprehensive modelling and comparative studies, a breakdown of touchdown patterns per runway may be helpful. Therefore, the ratio of rubber material deposited in the longitudinal direction of a specific touchdown zone and runway was calculated using Eq. (2). Considering the nature of the observed rubber spatial patterns, normal distribution-based fitting was introduced as shown in Fig. 8. In general, it is seen that touchdown zones L25, R25, R07, L07 show the highest rubber ratios compared to C07 and C25. Historical observations show that runway C07 is actually rarely used for landings and is rather dedicated more frequently for takeoffs. Also, it is noteworthy to indicate the potential irregularities, i.e. rubber spikes, especially in the touchdown R25. This can be explained by the higher concentration of rubber material on the intersecting high-speed exit path, which in the case of R25 is located at 500m. This increased rubber precipitates from tire treads as they rotate at high speeds during the runway rollout process.

$$\text{Rubber ratio} = \frac{1}{N_{rwy}} \sum_{k=1}^{N_{rwy}} \frac{A_{r,k}}{A_k} \tag{2}$$

where N_{rwy} is the amount of runway available scans, meanwhile $A_{r,k}$ stands for the area of rubber spots and A_k for the total area of touchdown zone both for a single scan k.

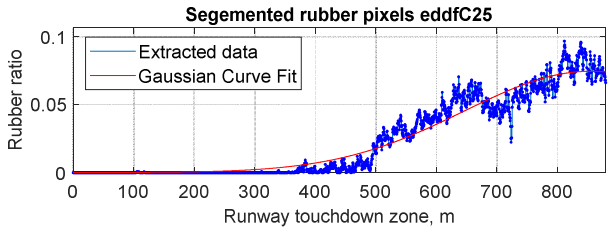

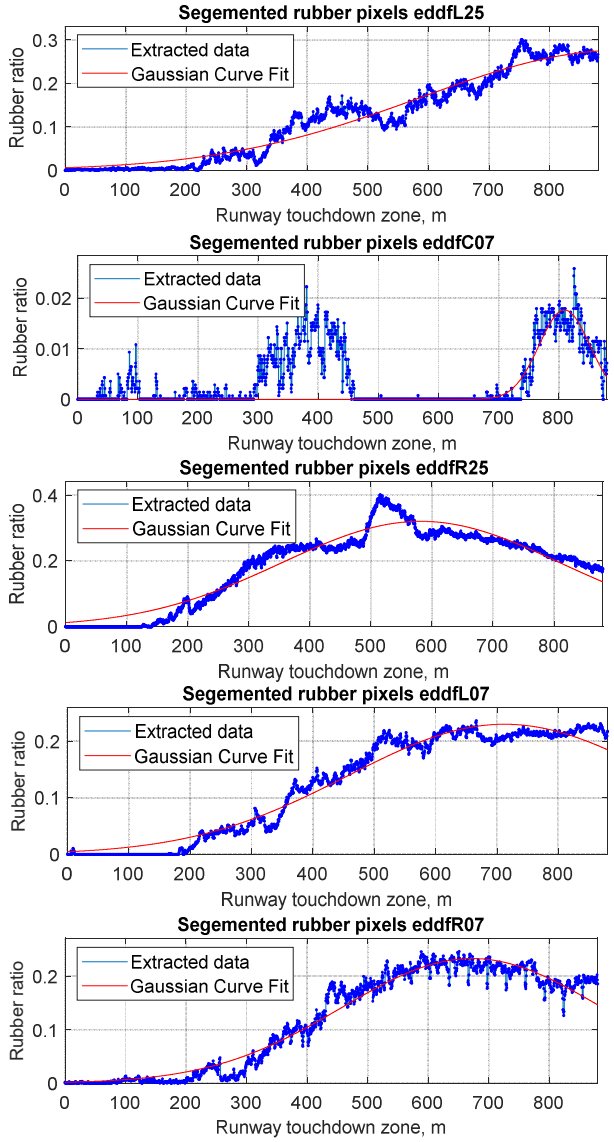

FIG. 8: Extracted and interpolated rubber ratios from EDDF runways

To obtain an airport-level descriptive model, rubber points from all EDDF arrival runways were aggregated and plotted in Fig. 9. Here, we observe how patterns on the runways scale add up to generate a unique pattern specific to the analyzed airport. The total rubber ratio distance-based pattern can be then empirically described using Gaussian interpolation method as follows,

$$\text{Rubber ratio} = k_1 \exp\left[-\frac{1}{k_3^2}(L_{TD} - k_2)^2\right] \quad (3)$$

where L_{TD} denotes the touchdown location. For the case of EDDF, the empirical coefficients are: $k_1 = 0.2185$, $k_2 = 721.9$ and $k_3 = 393.7$ all with 95% confidence bounds.

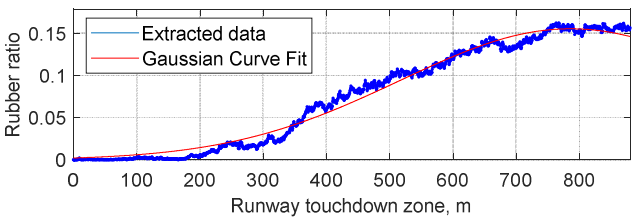

FIG. 9: Extracted and interpolated total rubber ratio for all landing runways at EDDF

3.3. Multiple airports-level observations

As an ultimate step, the developed analysis method is applied to extract and understand touchdown patterns from small clusters of airports and airfields. The main incentive towards the execution of such an analysis is the fact that airports differ in size and operational requirements/standards. In general, these standards are dictated by the dominant atmospheric, geographic, and ecological constraints. For illustration purposes, we consider a representative sample of six airports categorized in three subgroups based on the geographic location. Accordingly, Fig. 10 shows comparison between pairs of major airports in the USA, Europe and China, for each of which rubber ratios were accumulated and plotted. In this regard, few noteworthy observations deserve to be discussed. The first of which is related to EGLL airport in the UK, which demonstrates the highest concentration of rubber on its touchdown zones. On the other hand, EDDF in Germany and KJFK in USA are found to be showing the least amount of rubber ratio on their landing runways surfaces. The main explanation of this observation stims from the understanding of each airport runway throughputs. Since this information is difficult to obtain for each airport of interest, an observational approach is adopted. Consequently, the collected runways historical scans are exploited to infer relevant generic information. Accordingly, it is noticed that EDDF airport operates in total six touchdown zones two of which, namely C07 and C25, are large but usually assigned for takeoffs. In the case of KJFK, there are eight touchdown zones some of which seem to be less utilized than the others due to the governing atmospheric conditions. On the contrary, EGLL has only two runways with four touchdown zones which has to be therefore fully loaded by both takeoffs and landings. This explains the visually observed dense rubber material on EGLL and differences between peer airports. It also implies information on airports actual and maximum arrivals capacity and how arrivals and departures are runway-wise distributed in different airports during different operational times. It also indicates the frequency and quality of rubber removal operations at the analyzed airports.

In addition, it is noticed that touchdown phases at EDDF and ZGSZ are notably extended compared to USA airports. As for EDDF, the previously described operational procedures are relatable for explanation, while in the case of Chinese airports ZGSZ and ZGGG it is suggested that the considered nonstandard aiming points marking, i.e. three stripes distance coding-based, on both airport touchdown zones seems to incentivize pilots to avoid landing on the secondary aiming points, but rather aim to points closer to the main landing marking, at ~ 450m.

Another observation to note is related to the tendency of rubber distributions in EDDF towards a statistical mean aiming point around 800m. This appears to be a strong evidence of the strictness and conservativeness with the respect to noise abatement regulations enforcement at EDDF [25-23]. Furthermore, this observation predicts that future planned implementation of similar noise reduction measures on peer airports, e.g. KJFK, as reported in [24] will probably reflect similar landing patterns. Generalization of these noise-related approach requirements should be

then considered when designing and planning future capacity-constrained airports, because the resulting longer approaches may increase AROT.

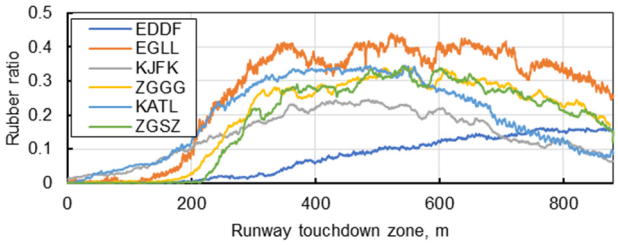

FIG. 10: Rubber ratios of different international airports

Instead of comparing airports of the same category, it is interesting to observe different patterns from different airport sets. In Fig. 11, it is seen that the mean aiming point correlates with the geographic location of the runway and its length especially in the absence of noise-related restrictions. In most cases, full touchdown process, i.e. main and nose wheels down, consumes the entire touchdown zone except for TNCM and LOWI, which is explained by the fact that these airports have shorter runways, only 2200m and 2000m, respectively, compared to 2800m or more in larger airports. In particular, pilots landing at TNCM seem to attempt strictly limiting touchdown to the available zone boundaries in order to avoid overruns to the surrounding sea water. For LOWI in Innsbruck, Austria, terrain and short runway combine together forcing pilots to shorten touchdown significantly. Consequently, these operational circumstances seem to encourage pilots to use available touchdown zone more effectively. However, this may also indicate fast or hard rotation phases, which cannot be studies in the scope of this paper.

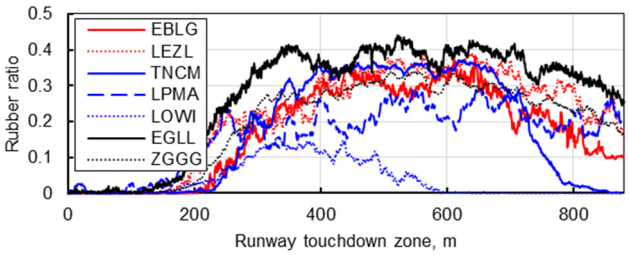

FIG. 11: Rubber ratios for six airports sorted by colors into the following three types: big airports (black); small airports (red) and airports with steep or short runways (blue)

4. DISCUSSION AND OPERATIONAL IMPLICATIONS

In this section, we provide and briefly discuss few exemplary applications of the developed method that may be helpful for understanding some aspects of landing operations. As noticed from the obtained results, the implementation of this method generates valuable measurements of runways surface texture properties and time-varying patterns. However, the method was not so far combined with an explanatory and predictive model. This becomes necessary to overcome the extreme need for abundant digital images to solve Eq. (3) for airports not included in the database. In fact, it is found that implemented Monte Carlo Gaussian Process -based approximation in Eq. (1) is extendable to express variations in $L_{TD,i}$ and ΔL, if their values are statistically or experimentally determined. Instead of inputting static variable for $L_{TD,i}$ imported from the literature, we can use APC speed limits and key approach parameters to an aircraft mass-point dynamic model according to,

$$L_{TD,i} = V_{ap,i} t_{ap,i} = h_{ap,i} / \tan(\gamma) \quad (4)$$

where $V_{ap,i}$ is the approach speed based on APC estimates, $t_{ap,i}$ is the given aircraft approach time, $h_{ap,i}$ is the final approach altitude over the threshold, and γ is the mean final approach and flare path angles. Considering $V_{ap,i}$ invariance in the context of actual operations [2], and the corresponding $t_{ap,i}$ statistical boundaries with a minimum of 7 seconds [2, 20], average $L_{TD,i}$ of any APC aircraft can be estimated. To simulate the entire annual fleet mixtures, ICAO suggestions regarding the merge of small low speed aircraft categories A and B are adopted for the sake of computations simplification [20]. Also, we consider the experimentally estimated ΔL = 225m. In Fig. 12, we simulate N=1.0×10^6 and output cumulative results per 500 axis bins of the touchdown zone length using a histogram plot. In result, it is seen that arrivals appear to share a mean touchdown point located at roughly 500m away from the runway threshold, which agrees with the previous data-driven estimates in Fig. 4 and resembles distribution patterns observed non-noise-constrained runways as in Fig. 10–11.

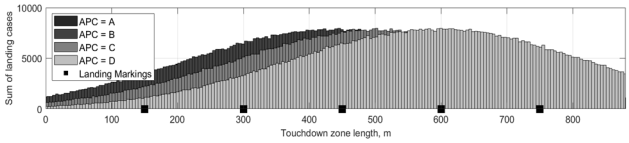

FIG. 12: Histogram of the simulated landing scenarios and the corresponding touchdown points

To reflect the effect of runway capacity-constraints coupled with low-noise landing procedures, increments in the approach time are assumed in the framework of two noise abatement strategies. The first strategy focuses on elevating approach paths of high-speed aircraft, namely B-D, because they are more responsible for noise emissions compared to the small-size low-speed general aviation airplanes approaching at speeds ≤ 90kts. Time increments for the simulated scenarios within this strategy are one and two seconds. For the second strategy, all approaching aircraft are inclusively commanded to follow higher paths and land at forwards displaced regions. Approach duration varies in this scenario based on the APC category. Note that this strategy is identical to the concept of multiple aiming points and displaced thresholds for noise abatements which has been proposed and successfully tested [25]. Results from both strategies simulations are presented in Fig. 13–14. Here, we see that the obtained distributions correlate with the observed cumulative trends and general patterns in airports such as EDDF and EGLL, see Fig. 10, and can explain their touchdown points displacement towards endpoints of the touchdown zone as a result of noise reduction measures. When equivalent touchdown and rubber zone areas to the measurement data are supposed, the same patterns in terms of rubber ratios can be also replicated.

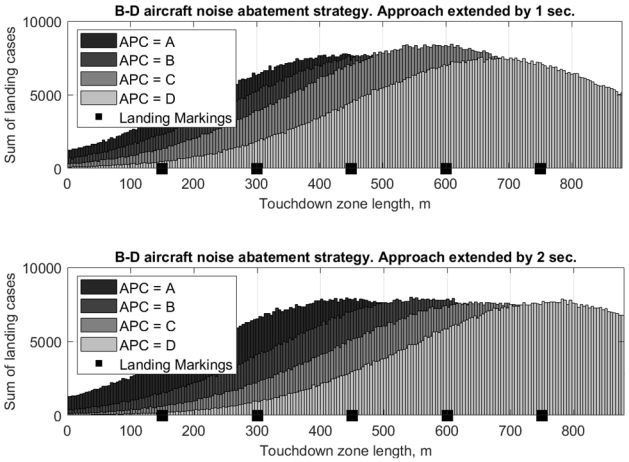

FIG. 13: Touchdown points distribution under the effect of high-speed aircraft noise abatement

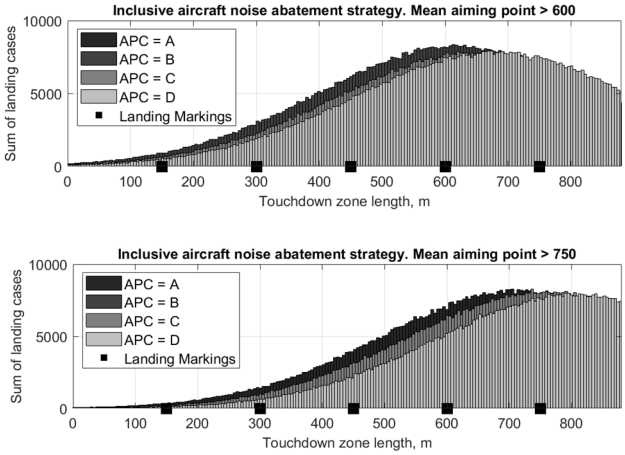

FIG. 14: Touchdown points distribution under the effect of displaced touchdown locations

The obtained knowledge of prolonged approach phases and displaced touchdown points implies further operational consequences with regard to AROT. It is common to assign close exits to the landing aircraft in order to increase runway throughput and accelerate runway vacation. Most normal day arrivals tend to vacate runways via exits located between 1600-2200m from the runway threshold to yield AROT 52±5 seconds [2, 26]. Awareness of the assigned exit and runway and airport design may influence pilots' decisions and delay touchdown as seen in [26]. However, pilots are generally recommended not to extend initial landing phases as they may lead to overshoot the assigned exits especially when operational situation is not in their favor. In fact, a similar consequence can be also predicted due to noise reduction-driven piloting behaviors, which may cause potential increase in AROT. In Fig. 15, it is shown that vacating through high-speed exits (30 deg.) located beyond 2250m require 60 seconds. This increases by 15–20 seconds in case a low-speed classic exit is used. For congested and capacity-constrained runways, this generates disturbance in the landing traffic, especially in case of approaches with minimum pairwise wake separations. To compensate the prolonged approach phase, landing aircraft must either apply higher braking power to vacate via the closest assigned exit or have the risk of exit overshooting and subsequent unexpected taxiing process to the next exit, which is completely undesired on busy runways. Application of higher braking force decreases brake discs lifetime and requires longer cooling time at parking gates, and of course, it worsens passenger travel experience. It also intensifies the unrecommended dependence on thrust reversers. Furthermore, future implementation of displaced touchdown points will reduce the need for first exits. This also points out to the necessary consideration of future large-scale noise mitigation measures effect on the currently recommended and standardized runway design assumptions, which for instance assume 250m and 450m mean touchdown points [20]. In addition, future landing and braking systems should be improved to consider the emerging operational and socio-ecological requirements and enhance accordingly runway occupancy efficiency.

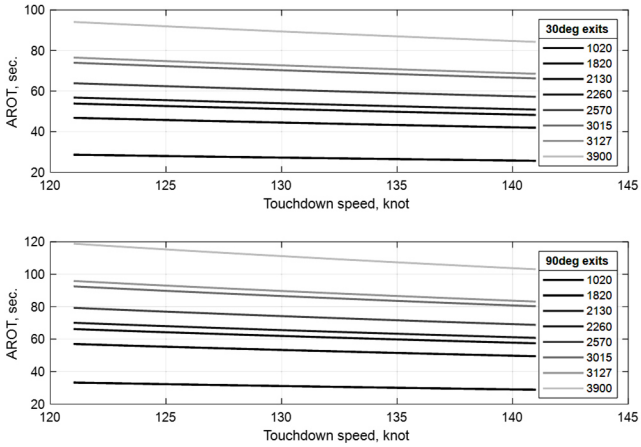

FIG. 15: AROT variations due to approach speed and exit parameters for normal day landings

Another interesting implication to infer from the analyzed touchdown patterns can be related to the possible prediction of dominant landing fleet aircraft types. In general, runways are designed for specific aircraft takeoff and landing operations. However, recognition of aircraft types that are actually operated on any runway during a given period will require proprietary surveillance and aircraft tracking system data, which is inaccessible for general academic research community. In the context of this work, it is found that observation of rubber material lateral distributions can be utilized to suggest prevalent aircraft types being frequently received by a runway of interest contingent on the availability of its satellite historical scans. In Fig. 16, we compute later rubber ratios from a few selected runways from different airports. Here, we observe correlations between runway length, width, and the amplitude of the wave-like lateral rubber distribution patterns. In the framework of aircraft mass point -like dynamics and operations, lateral rubber distribution should demonstrate Gaussian patterns with the mean value overlapping on the runway centerline. However, for realistic analyses aircraft detailed geometry cannot be neglected. Aircraft should ideally contact runway surface on its centerline, which aligns with the nose wheel and halves main landing wheels span. Due to nose wheel relative size and loading smallness, its rubber traces can be neglected. On the contrary, main landing gear assembly is larger and responsible of landing impact absorption, which results in multiple rubber point/tracks latterly distanced in accordance with the outer span length of the main landing gear. The result is the observed double bell-shaped patterns seen in Fig. 16. By calculating the distance between the peaks and bottoms, i.e. wavelength, we can match the obtained lengths with known aircraft main landing gear spans, a

sample of which is provided in Fig. 17. Accordingly, we notice that EGLL-R09 runway could serve all different kinds of small and large size aircraft. This is indeed expected since this runway is long (~3700m), which is the same for most other big airports. For smaller airports such as EDDM and LOWI, we observe shorter wavelengths implying smaller operated aircraft types. The slight distribution asymmetry noticed in Fig. 16 is the natural manifestation of the large-scale intrinsic stochasticity effect within such operations, which is for instance stimulated by strong crosswinds that force pilots to temporarily lose perfect heading and alignment with runway centerline.

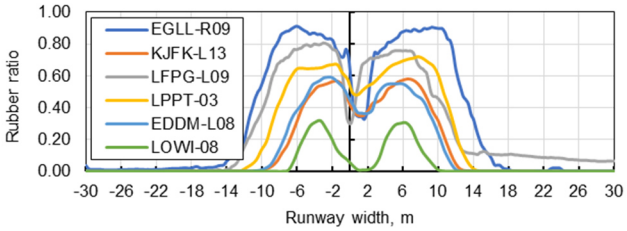

FIG. 16: Rubber ratio (lateral) for different runways and airports

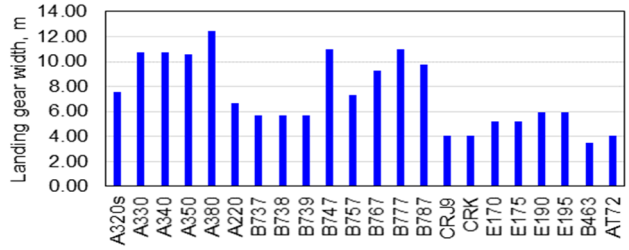

FIG. 17: Main landing wheel outer spans of most transport aircraft in service

Among the key limitations of the proposed method is the fact that it is well-suited for comprehensive and conceptual sampling-based analysis. Therefore, the obtained generalized patterns and relations are useful to validate or simulate air traffic and fleet operations within the air transportation systems, where specific aircraft dynamics are not of major interest. The other limitation is related to the quality and quantity of the available and collected satellite images. It is expected that a dedicated data collection campaign of tens or even hundreds of airports will help establish generic patterns worldwide and facilitate incorporation of machine learning techniques. In the case of rubber patterns usage for dominant landing aircraft types detection, the associated uncertainty needs enhancement as well. For instance, the width of rubber area does not take into account the effect of crosswind landings on the possible inflation of rubber area width. This means wide rubber zones will not necessarily correlate to large aircraft types. This application is however novel and sufficient for producing approximate data-driven predictions and gaining relevant preliminary understanding.

5. CONCLUSIONS AND FURTHER WORK

This paper presented a data-driven analysis method for extracting touchdown zone rubber patterns from satellite digital scans to help infer relevant operational implications. For this purpose, a set of 24 different airports was selected, satellite images of which were collected and analyzed using image processing techniques. The extracted rubber patterns were compared on the level of a single runway, an entire airport and a cluster of airports. Results have shown that rubber spots scattered on almost all landing runways can be used to detect and track time-varying piloting and landing trends on different airports and be able to derive generalized representations of the resulting touchdown points patterns, which can be then explained using Monte Carlo simulations under Gaussian Processes considerations. Effects of the ongoing pandemic and displaced landing points for noise abatement on approach and touchdown operations was explained. Furthermore, implications of these measures on runways efficiency were discussed. Besides, the possibility of this method implementation for recognizing arriving aircraft types was examined.

The present paper focused only on the landing process implications and application of the proposed method. However, further applications are foreseen. For instance, the method can be used for tracking and monitoring rubber removal operations quality and frequency monitoring for airports of abundant image database. Also, data-driven investigations of different runway landing markings and signs types and distancing parameters effect on landing patterns may be conducted. In addition, frequency and quality of these navigation signs re-painting activities can be assessed. All these applications enable independent local and international internal and external, i.e. non-contracted, authorities and institutions to monitor, track, and evaluate different airports operational standards and adherence to high safety and quality requirements by solely using free geoinformational data resources.

6. REFERENCES

[1] Eurocontrol. Airside, Airport and Runway Throughput. https://www.eurocontrol.int/project/airside-airport-and-runway-throughput, 2020.

[2] Meijers, N. P., & Hansman, R. J. A data-driven approach to understanding runway occupancy time. In AIAA Aviation 2019 Forum, Dallas, Texas, USA, 2019.

[3] Hu, J., Mirmohammadsadeghi, N., & Trani, A. Runway occupancy time constraint and runway throughput estimation under reduced arrival wake separation rules. *In AIAA Aviation 2019 Forum, Dallas, Texas, USA*, 2019.

[4] Eurocontrol. European Wake Turbulence Categorisation and Separation Minima on Approach and Departure (RECAT-EU), https://www.eurocontrol.int/archive_download/all/node/9681, 2018.

[5] Gerard W.H. et al. A Study of Normal Operational Landing Performance on Subsonic, Civil, Narrow-Body Jet Aircraft During Instrument Landing System Approaches. FAA. http://www.tc.faa.gov/its/worldpac/techrpt/ar077.pdf, 2007.

[6] Puranik, T. G., Harrison, E., Min, S., Jimenez, H., & Mavris, D. N. General Aviation Approach and Landing Analysis Using Flight Data Records. *In 16th AIAA*

Aviation Technology, Integration, and Operations Conference, Wichita, Kansas, USA, 2016.

[7] Cheng, A., & Ouyang, M. A. simulation study on identifying aircraft touchdown point by using in-flight recorded data. *AIAA Guidance, Navigation, and Control Conference, Toronto, Ontario Canada*, 2010.

[8] Olive, X., & Bieber, P. Quantitative Assessments of Runway Excursion Precursors using Mode S data. *In ICRAT-International Conference for Research in Air Transportation, Catalunya, Spain*, 2018.

[9] Parker, A., Gonzalez, L. F., & Trotter, P. Live detection of foreign object debris on runways detection using drones and AI. *In Proceedings of the 2022 IEEE International Aerospace Conference. Institute of Electrical and Electronics Engineers Inc,* 2021. https://eprints.qut.edu.au/227005/

[10] Hiba, A., Gáti, A., & Manecy, A. Optical navigation sensor for runway relative positioning of aircraft during final approach. *Sensors, 21(6), 2203*, 2021. https://doi.org/10.3390/s21062203

[11] Marianandam, P. A., & Ghose, D. Vision based alignment to runway during approach for landing of fixed wing UAVs. *IFAC Proceedings Volumes, 47(1), 470-476*, 2014. https://doi.org/10.3182/20140313-3-IN-3024.00197

[12] Akbar, J., Shahzad, M., Malik, M. I., Ul-Hasan, A., & Shafait, F. Runway detection and localization in aerial images using deep learning. *In 2019 Digital Image Computing: Techniques and Applications (DICTA), p. 1-8, IEEE*, 2019.

[13] Tripathi, A. K., Patel, V. V., & Padhi, R. Vision Based Automatic Landing with Runway Identification and Tracking. *In 2018 15th International Conference on Control, Automation, Robotics and Vision (ICARCV) (pp. 1442-1447). IEEE*, 2018.

[14] Moore, A. J., Schubert, M., Dolph, C., & Woodell, G. Machine vision identification of airport runways with visible and infrared videos. *Journal of Aerospace Information Systems, 13(7), 266-277*, 2016.

[15] Jiang, P., Li, K., & Li, Y. Airport Detection on Optical Satellite Images Using Machine Learning Method. *In 2020 Chinese Control and Decision Conference (CCDC) (pp. 3729-3734). IEEE*, 2020.

[16] Li, W., Xiang, S., Wang, H., & Pan, C. Robust airplane detection in satellite images. *In 2011 18th IEEE International Conference on Image Processing (pp. 2821-2824). IEEE*, 2011.

[17] Zhang, P., Niu, X., Dou, Y., & Xia, F. Airport detection on optical satellite images using deep convolutional neural networks. *IEEE Geoscience and Remote Sensing Letters, 14(8), 1183-1187*, 2017.

[18] Google. Google Earth Pro. https://www.google.com/intl/en/earth/versions/#earth-pro, 2022.

[19] ICAO. Aerodrome Design Manual, Part 2, Taxiways, Aprons, and Holding Bays. *International Civil Aviation Organization (ICAO)*. https://skybrary.aero/sites/default/files/bookshelf/3090.pdf, 2005.

[20] Schmid, P. Performance Margins. *Boeing Performance and Flight Operations Engineering Conference, Seattle, USA, 2007.* https://www.smartcockpit.com/docs/Performance_Margins.pdf

[21] Monk, H. Helen's Rules of Thumb. *FAA Technical Center Capacity Seminar*, 2006. https://www.faa.gov/airports/northwest_mountain/planning_capacity/media/airport-capacity-rules-of-thumb.pdf

[22] FRAPORT. Aircraft Noise - Active Noise Abatement. Frankfurt am Mein Airport (FRAPORT), 2022. https://www.fraport.com/en/environment/noise-abatement.html

[23] Zoltan Bazso. Active Noise Abatement at London Heathrow. Heathrow Airport, 2016. https://www.umwelthaus.org/media/9.icana2016_active_noise_abatement_heathrow.pdf

[24] Clare Secrist. New FAA Air Traffic Rules Aimed at Reducing Noise at JFK Airport. *WSHU*, 2020. https://www.wshu.org/news/2020-12-08/new-faa-air-traffic-rules-aimed-at-reducing-noise-at-jfk-airport

[25] Helmke, H., Hann, R., Uebbing-Rumke, M., Müller, D., & Wittkowski, D. Time-based arrival management for dual threshold operation and continuous descent approaches. *In 8th USA/Europe ATM Seminar, Napa, CA, USA*, 2009.

[26] Lim, Z. J., Goh, S. K., Dhief, I., & Alam, S. Causal effects of landing parameters on runway occupancy time using causal machine learning models. *In 2020 IEEE Symposium Series on Computational Intelligence (SSCI), 2713-2722*. IEEE, 2020.